Approximate Calculation and Measurement of the Pressure Distribution in Radial Flow of Molten Polymers Between Parallel Discs

HORST H. WINTER°

Department of Chemical Engineering and Rheology Research Center of the University of Wisconsin Madison, Wisconsin

The known generalized Newtonian fluid "power law" solution of the radial flow between parallel discs has been used to estimate the normal stress, the magnitude of inertia, and the temperature changes due to viscous dissipation. The flow near the wall has been found to be "nearly steady shear flow;" thus the three viscometric functions can be expected to describe the stress at the wall. Further away from the walls, however, the flow is very different from "steady shear flow."

The temperature field in the radial flow section depends on the dimensionless parameters Nahme number, Graetz number, and ratio of inner to outer radius, as well as on the thermal initial and boundary conditions.

Experimentally the radial pressure profiles for flow of three different polyethylenes and of one polystyrene have been studied. The measured pressure profiles are about 20 percent lower than the calculated ones from the "power law" solution. This discrepancy cannot yet be explained; the effects of normal stresses, of inertia, or of viscous heating in these experiments are too small to give a measurable effect.

INTRODUCTION

The disc-shaped cavity is a simple geometry for studying the molding-filling process in injection molding. The material enters in the center through a single circular tube and flows radially outwards between the parallel-disc surfaces (*Fig. 1*).

The assumptions made in the following analysis are

- $v = (v_r(r, z), 0, 0)$,
- $\rho =$ constant,
- Steady flow $(\partial/\partial t = 0)$,
- Rotational symmetry $(\partial/\partial\theta = 0)$, and
- Inertia terms in the equation of motion are negligible.

Additionally, it will be assumed later on, that the GNF "power law" solution describes the wall shear rate $\dot{\gamma}_{rz}(r, h/2)$ reasonably well.

Using the assumptions that $v_r(r, z)$ is the only nonzero velocity component and that the density is constant, one gets from the steady state equation of continuity

$$v_r = \frac{f(z)}{r} \qquad (1)$$

The rate of strain tensor in cylindrical coordinates is

$$\dot{\underline{\underline{\gamma}}} = \nabla \underline{v} + (\nabla \underline{v})^+ = \begin{bmatrix} -2r^{-2}f & 0 & r^{-1}f' \\ 0 & 2r^{-2}f & 0 \\ r^{-1}f' & 0 & 0 \end{bmatrix} \qquad (2)$$

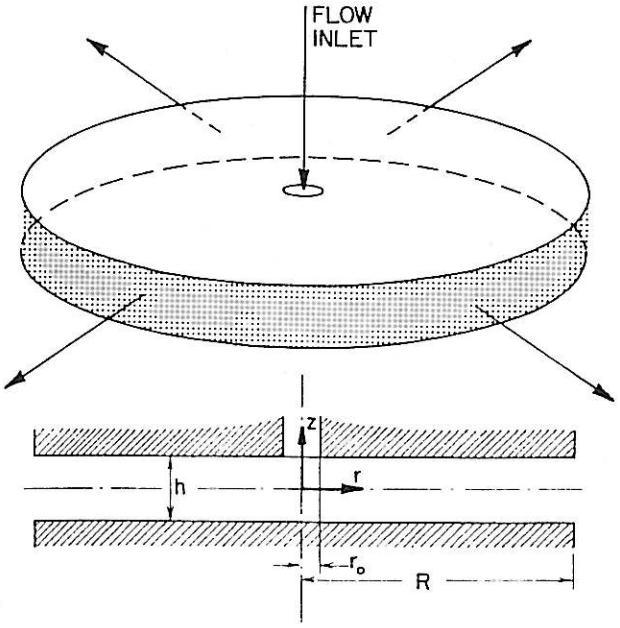

Fig. 1. Radial flow geometry.

° On leave from the Institut fur Kunststofftechnologie der Universitat Stuttgart, Boblingerstr. 70, 7 Stuttgart-1, West Germany.

with $f' = df/dz$. At the wetted disc surfaces ($z = \pm h/2$, $f(h/2) = 0$, $f'(h/2) \neq 0$) the material is being sheared only. Towards the middle ($0 < |z| < h/2$, $f(z) \neq 0$, $f'(z) \neq 0$) the elongational components $\dot{\gamma}_{rr}$ and $\dot{\gamma}_{\theta\theta}$ become more and more important, and in the center plane ($z = 0$, $f(0) \neq 0$, $f'(0) = 0$) there is elongational flow only (pure shear).

The equation of motion simplifies to

$$r\text{-component:}\quad 0 = -\frac{\partial p}{\partial r} - \frac{\partial \tau_{rr}}{\partial r} - \frac{\tau_{rr} - \tau_{\theta\theta}}{r} - \frac{\partial \tau_{rz}}{\partial z} \tag{3}$$

$$z\text{-component:}\quad 0 = -\frac{\partial p}{\partial z} - \frac{\partial \tau_{zz}}{\partial z} - \frac{1}{r}\frac{\partial}{\partial r}(r\tau_{rz}) \tag{4}$$

For calculating the velocity field v_r and the pressure p one has to choose a form of the stress tensor, which describes the rheological behavior of non-Newtonian liquids in radial flow. Because of the simplicity the GNF (generalized Newtonian fluid) with η given by the "power law" model (*Eq 5*), has been applied by a number of investigators (1-6), some of them using a numerical approach to include temperature effects and to tackle the unsteady mold filling problem (3-5). Laurencena and Williams (6) show experimentally that the "power law" model gives surprisingly good predictions for the radial pressure profile at the wall. The liquids they used had some elasticity $\left(\frac{\tau_{11} - \tau_{22}}{\tau_{12}} < 1 \text{ for } \dot{\gamma}_{12} < 1000\right)$. For more elastic materials (such as molten polymers), however, or at higher flow rates, one might expect significant deviations from the "power law" solution.

There seems to be no analysis available for fluids with large shear thinning effect and large elasticity as in molten polymers. Schwarz and Bruce (7) used a perturbation technique for studying small deviations from the Newtonian behavior of a Rivlin-Ericksen fluid including inertia effects. In their experiments they were aiming at the zero shear rate region. For high flow rates reportedly the spacing of the plates could not be maintained.

In a similar way, Piau and Piau (8) studied high Reynolds number flow of fluids with a characteristic time constant much smaller than the residence time in the radial flow section. They treated radial flow as if it were viscometric and showed a perturbation solution for a second-order fluid.

In the following, the GNF power law solution will be described briefly. Then it will be modified to include the normal stress components. The velocity field of the GNF power law solution will be used to estimate the normal stresses at the wall and their effect on the radial pressure profile at the walls. In addition the importance of inertia will be estimated.

GNF POWER LAW SOLUTION

In steady shear flow the shear-rate dependence of the viscosity is often described by a "power law"

$$\eta = m\,\dot{\gamma}^{n-1} \tag{5}$$

in which $\dot{\gamma} = \sqrt{1/2 \sum\sum \dot{\gamma}_{ij}^2}$. For molten polymers the power law exponent n usually has values between 0.2 and 0.5.

The additional assumptions for the GNF "power law" solution are

- The normal stress terms in the r-component of the equation of motion (*Eq 3*) cancel

$$\frac{\partial \tau_{rr}}{\partial r} + \frac{\tau_{rr} - \tau_{\theta\theta}}{r} \approx 0 \tag{6}$$

(Note that these terms sum sum to exactly zero for Newtonian fluids), and *Eq 3* simplifies to

$$0 = -\frac{\partial p}{\partial r} - \frac{\partial \tau_{rz}}{\partial z} \tag{7}$$

- The radial pressure gradient dp/dr is a function of r only, and
- $\dot{\gamma} = |\dot{\gamma}_{rz}|$, i.e. the other terms are negligible.

As reported (2, 6), using *Eqs 7* and *5* one gets the velocity

$$v_r = \frac{f(z)}{r}$$

$$f(z) = \overset{+}{(-)}\frac{Q}{2\pi h}\,\frac{2n+1}{n+1}\left[1 - \left(\frac{2z}{h}\right)^{\frac{1+n}{n}}\right] \tag{8}$$

and the pressure

$$p(r) - p(R) = \underbrace{\overset{+}{(-)}\left(\frac{2n+1}{n}\,\frac{Q}{\pi R h^2}\right)^n m}_{(\tau_{rz})_{w,R}}\,\frac{2R}{h(1-n)}\left[1 - \left(\frac{r}{R}\right)^{1-n}\right] \tag{9}$$

in which $(\tau_{rz})_{w,R}$ is the shear stress at the outer end of the upper wall. The sign in the small parentheses has to be used for converging radial flow respectively. Q is the volume flow rate ($Q > 0$ defined independent of flow direction), R is the outer radius, and h is the distance between the discs.

Figure 2 shows pressure profiles for different "power law" exponents. For the Newtonian fluid ($n = 1$) the pressure profile is a straight line on a semilogarithmic plot. With decreasing values of n the pressure drop gets smaller.

WALL STRESS DESCRIBED BY THE CRIMINALE-ERICKSEN-FILBEY (CEF) EQUATION (9)

The success of the GNF "power law" solution in describing the radial pressure distribution in polymer solutions (shown by ref. 6) might be explained by the shear stress term being much larger than the normal stress term (in *Eq 3*). But in spite of that, the shear stress τ_{rz} in radial flow can be expected to be very different from the calculated values τ_{rz} ($\dot{\gamma}$)

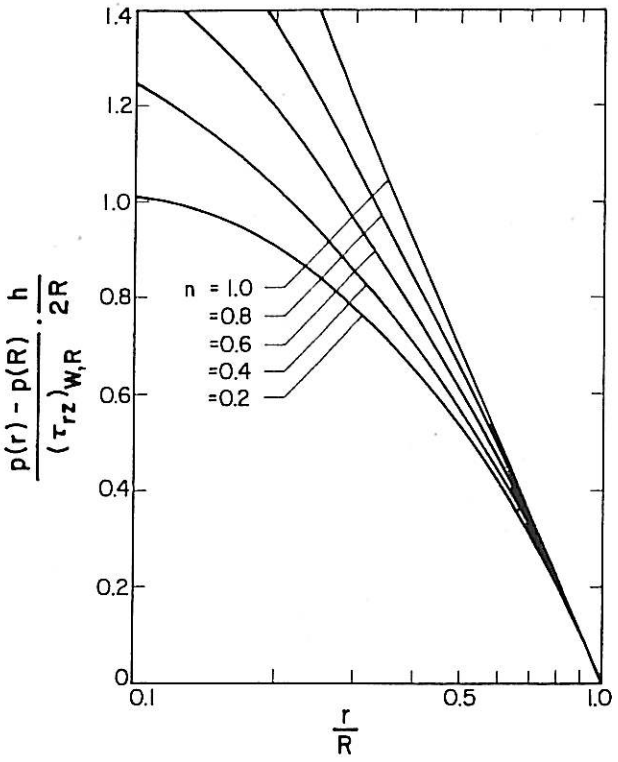

Fig. 2. Pressure profiles for GNF "power law" fluids in converging ($(\tau_{rz})_{w,R} < 0$) and diverging ($(\tau_{rz})_{w,R} > 0$) radial flow.

of the power law solution: a liquid element is subjected to varying shear stresses as it moves through the radial flow section. Thus, the flow is different from what is defined as "steady shear flow."

As an exception, however, the thin liquid layer closest to the walls is subjected to steady shear flow. This might be explained by looking at a fluid element slowly moving in a small distance δ from the wall (*Fig. 3*). The velocity field is assumed to be constant with time ($\partial/\partial t = 0$), but changing with position. Close to the wall the changes in flow direction are much smaller than perpendicular to it. As the fluid element moves along slowly, it is being deformed at relatively high shear rates $\dot{\gamma}$ ($\partial v_1/\partial x_2 >> \partial v_1/\partial x_1$). Because the fluid moves slowly, the changes in $\dot{\gamma}$ are very slow, too; this type of flow is called "nearly steady shear flow" or "nearly viscometric flow." In the limiting case $\delta \to 0$ in *Fig. 3*), a liquid element sitting at the wall is

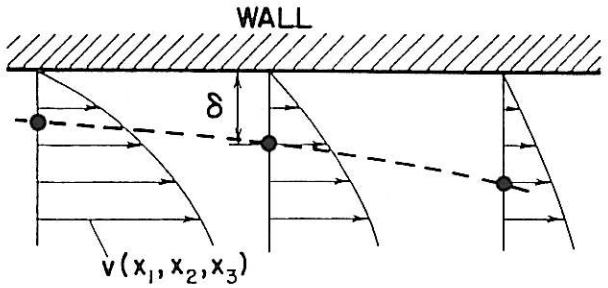

Fig. 3. Sketch of a velocity field near a wall and the path of a fluid element in a small distance δ from the wall.

deforming at a constant rate, which depends on its radial position.

$$\dot{\gamma}_{rz}\left(r, \frac{h}{2}\right) = \frac{f'_w}{r} \equiv \dot{\gamma}_w(r) \tag{10}$$

(Note that this argument is valid for channel flow in any geometry as long as (a) the fluid wets the wall and (b) the velocity stays constant with time.)

The extra stress tensor $\underline{\tau}$ at the upper wall is defined by the viscometric functions η, θ, and β.

$$(\tau_{rz})_w = -\eta\,\dot{\gamma}_w, \quad \eta \approx m\left|\dot{\gamma}_w\right|^{n-1} \tag{11}$$

$$(\tau_{rr} - \tau_{zz})_w = -\theta\,\dot{\gamma}_w^2, \quad \theta \approx m'\left|\dot{\gamma}_w\right|^{n'-2} \tag{12}$$

$$(\tau_{zz} - \tau_{\theta\theta})_w = -\beta\,\dot{\gamma}_w^2, \quad \beta \approx m''\left|\dot{\gamma}_w\right|^{n''-2}$$

$$m, m', n, n', n'' > 0; \quad m'' < 0,$$

which will be described approximately by a power law throughout the following calculation.

The r-component of the equation of motion may be evaluated at the wall. After adding $\partial\tau_{rr}/\partial r$ on both sides, *Eq 3* can be integrated over r to give

$$\int_r^R \frac{\partial}{\partial r}(p + \tau_{zz})\mathrm{d}r =$$

$$-\int_r^R \left[\frac{\partial}{\partial r}(\tau_{rr} - \tau_{zz}) + \frac{1}{r}(\tau_{rr} - \tau_{\theta\theta})\right]\mathrm{d}r$$

$$-\int_r^R \frac{\partial \tau_{rz}}{\partial z}\mathrm{d}r \tag{13}$$

Using the power law form of the viscometric functions, one can integrate the normal stress terms and the shear stress term to get the solution for the normal stress $p + \tau_{zz}$ perpendicular to the wall:

Normal stress terms

$$\int_r^R \left[\frac{\partial}{\partial r}(\tau_{rr} - \tau_{zz})_w + \frac{1}{r}(\tau_{rr} - \tau_{\theta\theta})_w\right]\mathrm{d}r$$

$$= (\tau_{rr} - \tau_{zz})_{w,R}\left[1 - \frac{r^{-n'}}{R}\right] + \int_r^R (\tau_{rr} - \tau_{\theta\theta})_w \frac{\mathrm{d}r}{r}$$

$$= \frac{1 - n'}{n'}(\tau_{rr} - \tau_{zz})_{w,R}\left[\left(\frac{R}{r}\right)^{n'} - 1\right]$$

$$+ \frac{1}{n''}(\tau_{zz} - \tau_{\theta\theta})_{w,R}\left[\left(\frac{R}{r}\right)^{n''} - 1\right] \tag{14}$$

Shear stress term

$$\int_r^R \frac{\partial}{\partial z}(\tau_{rz})_w \mathrm{d}r = -m\frac{f'_w}{|f'_w|}\frac{\partial}{\partial z}|f'_w|^n \int_r^R r^{-n}\mathrm{d}r$$

$$= (\tau_{rz})_{w,R}\frac{nR}{1-n}\left[1 - \left(\frac{r}{R}\right)^{1-n}\right]\frac{f''_w}{f'_w} \tag{15}$$

The integrated r-component of the equation of motion becomes

$$(p + \tau_{zz})_{w,r} - (p + \tau_{zz})_{w,R}$$

$$= (\tau_{rz})_{w,R} \frac{nR}{1-n} \frac{f''_w}{f'_w} \left[1 - \left(\frac{r}{R} \right)^{1-n} \right]$$

$$+ (\tau_{rr} - \tau_{zz})_{w,R} \frac{1-n'}{n'} \left[\left(\frac{R}{r} \right)^{n'} - 1 \right]$$

$$+ (\tau_{zz} - \tau_{\theta\theta})_{w,R} \frac{1}{n''} \left[\left(\frac{R}{r} \right)^{n''} - 1 \right] \quad (16)$$

In the sign convention, which has been used in this analysis, the shear stress τ_{rz} is positive for outward flow and negative for inward flow. The first normal stress difference is always negative, whereas the second normal stress difference is approximately one-fourth the first normal stress difference.

For *diverging* radial flow ($f'_w < 0$; $0 < (\tau_{rz})_{w,R}$) the CEF equation with power law material functions predicts smaller drops than one would expect from the GNF "power law" solution (*Eq 9*). Thus the normal stress effects assist in the injection molding process. From the estimate (*Eq 17*) one expects large normal stress effects in very elastic liquids, at large flow rates, or at large values of h/R.

For *converging* radial flow ($0 < f'_w$; $(\tau_{rz})_{w,R} < 0$), however, the normal stress terms add to the shear stress term, and one gets a pressure drop larger than one would expect from the GNF "power law" solution. The normal stress distribution at the wall $(p + \tau_{zz})_{w,r}$ contains the wall pressure $p(r)$ of the GNF "power law" solution (*Eq 9*) as the first term at the right hand side. The normal stress terms (*Eq 14*) are of negligible influence if

$$\frac{f'_w}{nRf''_w} \left[\left(\frac{R}{r_0} \right)^{n'} \frac{1-n'}{n'} \left(\frac{\tau_{rr} - \tau_{zz}}{\tau_{rz}} \right)_{w,R} + \left(\frac{R}{r_0} \right)^{n''} \frac{1}{n''} \left(\frac{\tau_{zz} - \tau_{\theta\theta}}{\tau_{rz}} \right)_{w,R} \right] << 1 \quad (17)$$

For small deviations from the GNF "power law" solution, the wall shear stress at the outer radius $(\tau_{rz})_{w,R}$, and the first and the second normal stress differences at the wall and at the outer radius $(\tau_{rr} - \tau_{zz})_{w,R}$, $(\tau_{zz} - \tau_{\theta\theta})_{w,R}$ can be evaluated approximately by introducing the velocity field given in *Eq 8* into the viscometric functions (*Eqs 11* and *12*).

$$(\tau_{rz})_{w,R} \approx \overset{+}{(-)} m \left(\frac{Q}{\pi h^2 R} \frac{2n+1}{n} \right)^n$$

$$(\tau_{rr} - \tau_{zz})_{w,R} \approx -m' \left(\frac{Q}{\pi h^2 R} \frac{2n+1}{n} \right)^{n'} \quad (18)$$

$$(\tau_{zz} - \tau_{\theta\theta})_{w,R} \approx -m'' \left(\frac{Q}{\pi h^2 R} \frac{2n+1}{n} \right)^{n''}$$

The wall shear rate of the GNF "power law" solution is

$$\dot{\gamma}_w = \frac{f'_w}{r} = \frac{nh}{2} \frac{f''_w}{r} = \overset{-}{(+)} \frac{Q}{\pi h^2 R} \frac{2n+1}{n} \quad (19)$$

If the actual wall pressure differs very much from the GNF "power law" solution (*Eq 9*), one might expect that the actual wall shear rate is not described accurately enough by the velocity field given in *Eq 8*. In this case it seems unavoidable to seek a complete solution of the radial flow problem by means of a constitutive equation which is valid in the whole radial flow channel.

ESTIMATE OF INERTIA

Up to this point the effect of inertia has been assumed to be negligible. But at high flow rates, where normal stress effects become important, inertia effects might also be of influence. Thus a criterion is needed for estimating the magnitude of the inertia.

The r-component of the equation of motion with the inertia term included for steady radial flow is

$$\rho v_r \frac{\partial v_r}{\partial r} = -\frac{\partial p}{\partial r} - \frac{\partial \tau_{rr}}{\partial r} - \frac{\tau_{rr} - \tau_{\theta\theta}}{r} - \frac{\partial \tau_{rz}}{\partial z} \quad (20)$$

The inertia term might be transformed using *Eq 1* and then approximated by averaging the velocity

$$\rho v_r \frac{\partial v_r}{\partial r} = -\rho \frac{v_r^2}{r} \approx -\frac{\rho}{r} \left(\frac{Q}{2\pi r h} \right)^2$$

The integration of the equation of motion leads to

$$(p + \tau_{zz})_{w,r} - (p + \tau_{zz})_{w,R}$$

$$= (\tau_{rz})_{w,R} \frac{nR}{1-n} \frac{f''_w}{f'_w} \left[1 - \left(\frac{r}{R} \right)^{1-n} \right]$$

$$+ (\tau_{rr} - \tau_{zz})_{w,R} \frac{1-n'}{n'} \left[\left(\frac{R}{r} \right)^{n'} - 1 \right]$$

$$+ (\tau_{zz} - \tau_{\theta\theta})_{w,R} \frac{1}{n''} \left[\left(\frac{R}{r} \right)^{n''} - 1 \right]$$

$$+ \frac{\rho}{2} \left(\frac{Q}{2\pi R h} \right)^2 \left[\left(\frac{R}{r} \right)^2 - 1 \right] \quad (21)$$

By comparing the inertia term and the shear stress term in *Eq 21* one can see that inertia is negligible if

$$\frac{\rho f'_w}{R f''_w (\tau_{rz})_{w,R}} \left(\frac{Q}{2\pi r_0 h} \right)^2 << 1 \quad (22)$$

f'_w, f''_w, and $(\tau_{rz})_{w,R}$ can be estimated from *Eq 18* and *Eq 19*. The dimensionless group can be understood as a Reynolds number for radial flow. If this criterion shows that inertia is important, a solution of *Eq 20* without averaging of the velocity field should be sought. For Newtonian fluids such solutions have been given in the literature (10, 11).

VISCOUS HEATING

The temperature field in radial flow is determined (1) by convection in r-direction, (2) by conduction in z-direction, and (3) by viscous dissipation. Due to the small thermal diffusivity of polymers, the heat conduction in flow direction can be neglected compared to the convection. For an incompressible fluid

the equation of energy in terms of the fluid temperature T is

$$\rho c v_r \frac{\partial T}{\partial r} = k \frac{\partial^2 T}{\partial z^2} + \eta \left(\frac{\partial v_r}{\partial z} \right)^2 \qquad (23)$$

The elongational contribution in the dissipation term is being neglected. The temperature dependence of the viscosity is described by an exponential function

$$\eta(\dot{\gamma}, T) = \eta(\dot{\gamma}, T_o) \cdot \exp[-b(T - T_o)] \qquad (24)$$

$b = -1/\eta \, (\partial \eta / \partial T)_{\dot{\gamma}}$ is the temperature coefficient of the viscosity.

For defining the dimensionless parameters, a reference velocity $\bar{v}_r$ and a reference viscosity $\bar{\eta}$ are defined. The reference velocity has been chosen to be the outer radius R divided by the average residence time in the radial flow section

$$\bar{v}_r = \frac{Q}{\pi R h} \qquad (25)$$

and the reference viscosity has been chosen at $T = T_o$ and at $\dot{\gamma} = \bar{v}_r/h$

$$\bar{\eta} = \eta \left(T_o, \frac{\bar{v}_r}{h} \right) \qquad (26)$$

The equation of motion (*Eq 7*) and the equation of energy (*Eq 23*) are coupled through the temperature dependent viscosity. The extent of the coupling increases with the value of the Nahme number

$$\mathrm{Na} = \frac{b \bar{v}_r^2 \bar{\eta}}{k} \qquad (27)$$

which compares the dissipation term and the conduction term in *Eq 23*. For small values of Na (Na < 0.5) the dissipation is very small, and experiments can be performed under conditions which are practically isothermal; the coupling between the equation of motion and the equation of energy can be neglected.

By comparing the convection term with the conduction term of *Eq 23* one gets the Graetz number

$$\mathrm{Gz} = \frac{h^2 \bar{v}_r}{aR} \qquad (28)$$

A large value of Gz means that heat convection in flow direction is more important than conduction towards the walls; on the other side, a small value of Gz means that the wall temperatures determine the fluid temperatures.

The velocity field is singular at $r = 0$. For small values or r_o/R the viscous dissipation in the entrance section ($r \approx r_o$) is very large, even at small Na.

One gets a system of two nonlinear partial differential equations (*Eqs 7* and *23*) and an integral for the volume flow rate at each radial position. It has been solved by an iterative implicit difference method.

For the demonstration of some results of the calculation, the wall temperatures and the inlet temperatures are assumed to be constant (equal to T_o). For the analysis of experimental results, the measured values for the temperatures are the initial and boundary conditions in the numerical program.

The influence of viscous dissipation on the pressure profile is shown in *Fig. 4*. The upper curve corresponds to isothermal flow of a GNF "power law" fluid (*Eq 9*). Any temperature increase (due to viscous dissipation in this case) lowers the pressure profile. The temperature effects are the largest at large values of Na and small values of Gz. For small values of Gz the residence time of the fluid is long enough to conduct most of the generated heat towards the isothermal walls; at large Gz, the heat of dissipation is convected out of the gap very rapidly.

The developing temperature profile (see *Fig. 5*) is dominated by convection and viscous dissipation, at first. The fluid temperatures increase in flow direction, and the temperature gradients towards the walls and towards the middle get steeper and steeper. The flow, however, slows down in r-direction ($v_r \sim r^{-1}$), and the conduction towards the walls becomes dominating. The fluid temperatures decrease again, since isothermal walls have been assumed. The temperatures in the center plane level off to the temperatures of the outer regions.

EXPERIMENTS

Experiments have been performed by the author together with Bertsch (12) at the Institut für Kunststofftechnologie der Universität Stuttgart.

The experimental set up is described in *Figs. 6* and *7*. A single screw extruder (with a mixing ele-

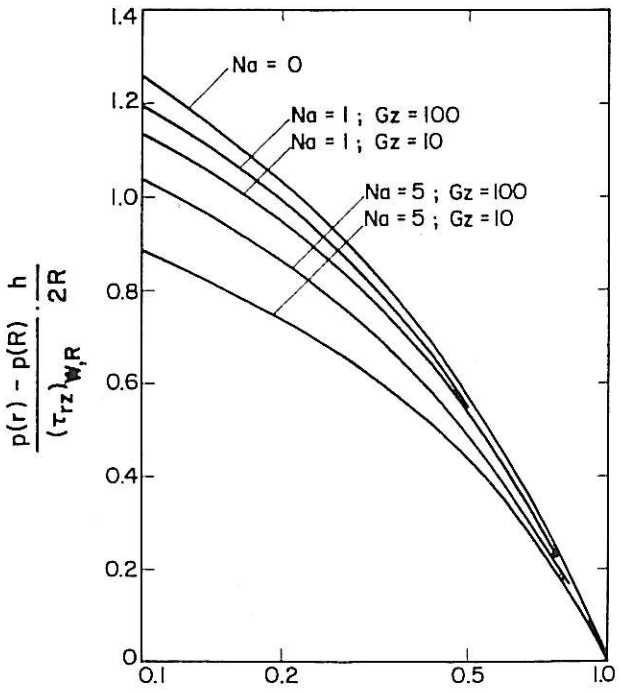

Fig. 4. Temperature effects on the radial pressure profiles; $n = 0.4$; $r_o/R = 0.05$. $(\tau_{rz})_{w,R}$ is calculated using Eq 18 and $m(T_o)$.

ment on the tip of the screw) supplies a molten polymer of uniform temperature. The molten polymer flows through a converging canal and through a single pipe ($d = 0.3$ cm, $l/d = 8$) into the center of the radial flow section. After passing the radial flow section, the material flows radially inward again through 16 radial channels (equally distributed on the circumference) and leaves the die through a single pipe. The flow rate in the radial flow section has been varied by changing the speed of rotation

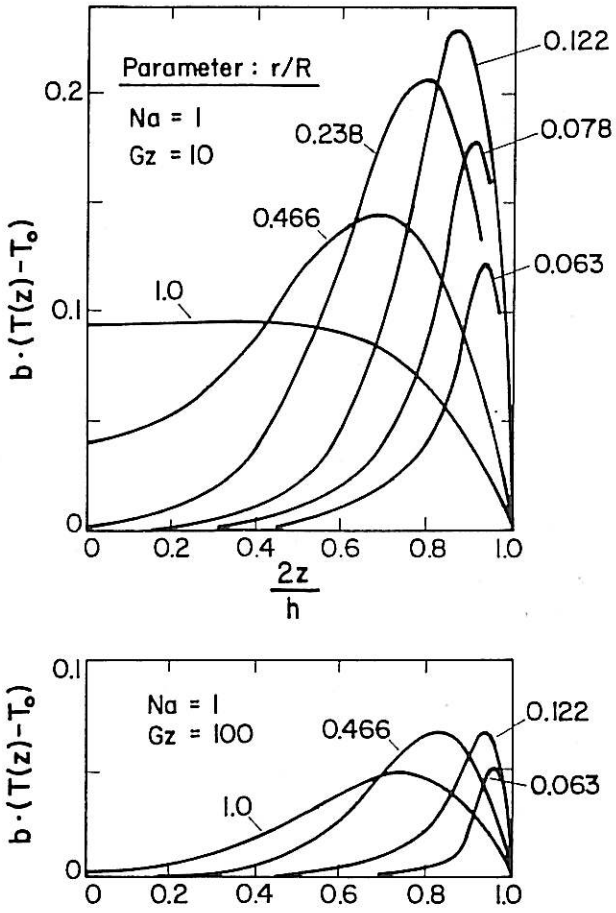

Fig. 5. Developing temperature profile in radial flow; $n = 0.4$; $r_0/R = 0.05$; $Na = 1$; $Gz = 10$ and $Gz = 100$; constant inlet and wall temperature.

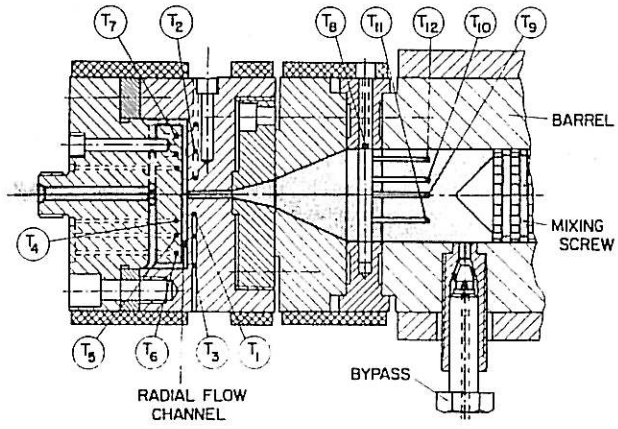

Fig. 6. Setup for radial flow experiments.

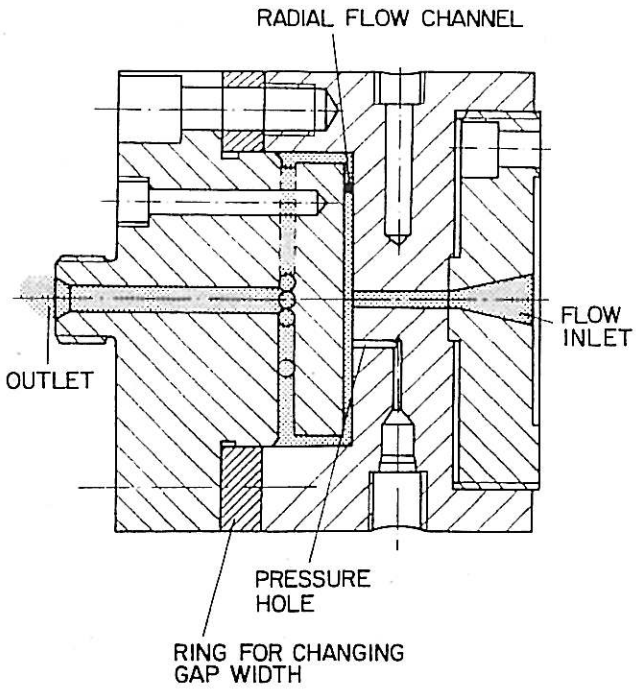

Fig. 7. Radial flow die.

of the extruder screw and by opening the bypass. The mass flow rate has been measured and then converted into a volume flow rate using specific volume data of Hellwege, Knappe, and Lehmann (13). The temperature is being measured at the wall of the radial flow section (T1-T7) and in the slow flowing polymer (T8-T12) before it enters the converging channel. The pressure is being measured by means of pressure transducers in holes at 6 radial positions ($r_6 = 3.2$ cm; $r_1/r_6 = 0.125$; $r_2/r_6 = 0.281$; $r_3/r_6 = 0.500$; $r_4/r_6 = 0.719$; $r_5/r_6 = 0.875$). The gap width is adjustable through distance rings ($h_1 = 0.0385 \pm 0.0012$ cm; $h_2 = 0.0895 \pm 0.0012$ cm; $h_3 = 0.1885 \pm 0.0012$ cm).

The accuracy of the measurements is ± 1.7 percent for the mass flow rate, ± 1.5 percent for the pressures, and ± 0.2°K for the temperatures.

The shear-dependent viscosities, measured by Robens (14), of the molten polymers used are listed in *Table 1*. Unfortunately, no normal stress data is available.

Table 1. Power Law data (14) of Molten Polymers. Range of Shear Rates: $60 < \dot{\gamma} < 1200$ sec^{-1}

Polymer	T, °C	m Nm^{-2} sec^n	n
Low-density polyethylene (Lupolen 1800H, BASF)	170	1.387×10^4	0.370
	190	1.087×10^4	0.379
High-density polyethylene, low molecular weight (Lupolen 3035K, BASF)	170	1.286×10^4	0.400
	190	0.908×10^4	0.435
High-density polyethylene, high molecular weight (Hostalen GF 4760, Hoechst)	250	1.734×10^4	0.417
	270	1.168×10^4	0.485
Polystyrene (SB 475K, BASF)	190	4.208×10^4	0.222
	210	2.654×10^4	0.250

Table 2. Data of Radial Flow Experiments

Polymer and number	Q, $cm^3\ sec^{-1}$	h, cm	T_o, °C	$(p + \tau_{zz})_{r_i}$, $10^5\ Nm^{-2}$					
				r_1	r_2	r_3	r_4	r_5	r_6
1800H									
1	3.45	0.0385	190.0	273.7	220.3	162.3	107.3	71.0	46.9
2	1.71	0.0385	182.5	236.8	186.0	131.5	88.7	58.7	38.3
3	0.86	0.0385	179.0	188.5	147.3	103.8	69.7	44.7	28.8
4	8.20	0.0895	187.5	132.4	113.3	92.4	78.6	65.8	57.5
5	4.03	0.0895	177.5	110.6	93.8	77.3	64.6	53.9	47.2
6	2.06	0.0895	180.5	86.0	73.1	59.5	49.7	40.8	36.3
7	16.04	0.1885	179.6	93.2	85.8	78.6	74.8	70.1	68.3
8	7.84	0.1885	174.0	80.2	71.7	67.2	63.4	59.3	58.3
9	4.21	0.1885	169.5	68.3	61.5	57.2	53.8	50.1	49.5
3035K									
10	3.55	0.0385	180.0	286.1	223.7	157.0	99.3	65.3	39.8
11	1.81	0.0385	179.5	221.9	172.5	120.3	75.3	48.5	29.5
12	0.84	0.0385	180.0	162.8	122.4	86.1	52.6	32.8	18.2
13	8.23	0.0895	176.0	130.5	110.1	89.5	71.0	59.6	52.2
14	4.11	0.0895	179.5	99.3	82.4	67.1	52.6	43.9	38.5
15	2.07	0.0895	180.0	72.2	57.9	49.1	37.5	29.6	27.7
16	8.26	0.1885	180.0	70.6	64.5	57.9	54.3	50.8	50.4
17	4.20	0.1885	182.0	52.4	47.3	44.9	39.8	36.9	37.5
GF 4760									
18	1.03	0.0385	250.0	373.0	264.3	188.7	116.9	75.9	44.5
19	0.49	0.0385	259.0	282.5	188.9	133.8	80.8	51.8	29.6
20	0.25	0.0385	251.0	226.0	143.4	100.5	60.2	37.7	21.4
21	2.51	0.0895	247.5	152.8	129.4	105.0	81.2	69.1	59.3
22	1.28	0.0895	255.0	118.7	99.9	79.9	61.6	52.0	44.1
23	4.66	0.0895	256.0	195.0	167.2	135.2	105.9	91.6	78.1
24	5.39	0.1885	257.0	112.0	103.8	96.3	86.5	84.6	80.6
25	2.80	0.1885	259.0	80.2	73.8	69.3	61.8	60.4	57.7
26	1.34	0.1885	255.0	56.1	51.2	45.9	43.0	42.0	40.0
SB 475K									
27	0.70	0.0385	182.0	260.0	213.5	162.5	110.3	79.1	54.9
28	0.34	0.0385	182.0	205.6	166.8	126.4	85.0	58.4	39.4
29	0.21	0.0385	184.0	183.3	148.5	111.2	72.8	49.8	33.2
30	1.84	0.0895	181.0	148.9	132.6	114.0	91.8	79.5	70.6
31	0.96	0.0895	181.0	122.2	108.1	92.4	73.0	62.6	55.7
32	0.42	0.0895	181.0	91.2	79.3	68.3	53.2	44.7	39.8
33	4.01	0.1885	226.0	56.6	51.2	49.4	42.6	40.0	39.8
34	1.90	0.1885	202.0	53.0	48.6	45.6	39.2	37.0	36.4
35	1.10	0.1885	180.0	75.4	70.2	66.4	58.0	54.4	53.2
36	0.73	0.0385	190.0	215.6	176.8	133.4	88.4	61.8	41.6
37	0.72	0.0385	200.0	182.4	147.6	109.6	72.4	46.6	32.4
38	0.73	0.0385	210.5	159.6	128.4	95.0	61.6	40.8	26.6

The measured "pressures" $(p + \tau_{zz})_{r_i}$ are listed in *Table 2*; the pressure profiles (normalized with the calculated wall shear stress (*Eq 18*) at the outer radius) are shown in *Figs. 8a-d*. The measured pressures are about 20 percent below the calculated values of the isothermal GNF power law solution.

DISCUSSION OF THE EXPERIMENTS

Normal Stress Effects

In a recent publication, Bird, Hassager and Abdel-Khalik (15) suggest a method of calculating the first normal stress coefficient $\theta(\dot{\gamma}^2)$ from viscosity data. For a number of fluids (including molten low-density polyethylene) these calculated values agree with experimental data in the literature. In the following, this method will be applied to get normal stress data for the low density polyethylene (Lupolen 1800H) used in the radial flow experiments. The zero shear rate viscosity η_o needed for this calculation will be taken from a study by Meissner (16) on a low-density polyethylene of the same brand. For shear rates above $4 sec^{-1}$ the temperature dependent viscosities of the two polyethylenes are practically identical; this suggests that the zero viscosities might be the same, too. The zero viscosities and the calculated values m' and n' are shown in *Table 3*.

Evaluation of the normal stress terms in *Eq 16* (by assuming $m'' = -1/4\ m'$, $n'' = n'$) gives pressure values, which are 0.1-1 percent below the GNF power law solution.

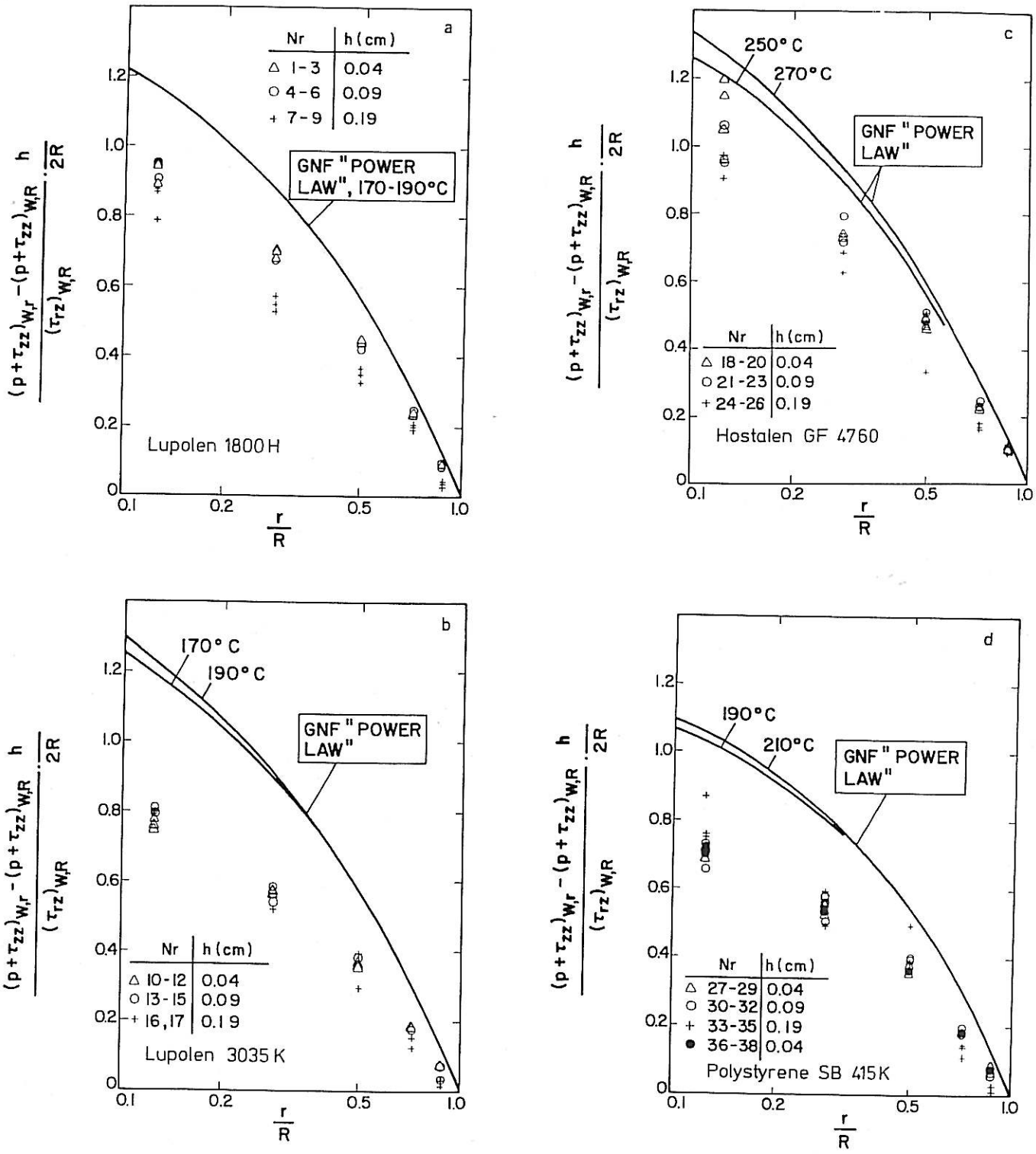

Fig. 8. Comparison of measured radial pressure profiles with the corresponding isothermal power law solution. (a) low-density PE (Lupolen 1800H, BASF); (b) high-density PE, low molecular weight (Lupolen 3035K, BASF); (c) high density PE, high molecular weight (Hostalen GF 4760, Hoechst); and (d) polystyrene (SB 475K, BASF). $(\tau_{rz})_{w,R}$ is calculated using Eq 18 and $m(T_o)$.

Pressure Hole Error Due to Normal Stresses

The systematic error p_H in the pressure measurement due to the pressure holes can be estimated by means of a formula derived by Higashitani and Pritchard (17).

$$p_H \approx \frac{n}{3}(\tau_{rr} - \tau_{zz})_w \qquad (29)$$

For the low-density polyethylene the actual pressure drop is about 0.3-1.3 percent larger than in the data given in *Table 2*.

Inertia

Application of *Eq 22* shows that inertia is negligible for all experiments.

Table 3. Zero Shear Rate Viscosity; Normal Stress Data Calculated from Viscosity Data Using a Method Suggested in Reference 15 (m′ and n′ Defined in Eq. 12) Polymer: Lupolen 1800H

T, °C	η_o, Nm^{-2} sec (16)	m′, Nm^{-2} sec^n	n′
170	2.04×10^4 (interpolated)	3.3×10^4	0.40
190	1.05×10^4	2.7×10^4	0.40

Viscous Heating

During the performance of the experiments significant viscous dissipation has been observed, and the lowering of the viscosity due to temperature raises diminishes the value of the radial pressure drop. The temperature of the molten polymer coming from the extruder screw has been quite uniform ($\Delta T < 0.5°K$). In the radial flow section, however, the wall temperature could not be maintained constant ($\Delta T < 5°K$), which means that the melt temperatures differ even more from the initial temperature level. For estimating the magnitude of the viscous dissipation, the wall temperatures are taken as thermal boundary conditions. To get the temperature distribution at the entrance of the radial flow section, the developing temperature field in the feed pipe ($\phi 2r_o$) is being calculated with an existing numerical program (18). Corresponding temperatures at the exit of the pipe and at the entrance to the radial flow section are calculated by assigning them to the same value of the stream function in the two flow geometries.

The values of the Nahme numbers between 0.01 and 0.43 show that dissipation does not influence the pressure profile very much. The Graetz number has values between 0.2 and 33.3 The ratio of the radii is $r_o/R = 0.048$.

Altogether, the normal stress effects and the effects of viscous heating show the right sign for bringing experimental values and analytical solution closer together. But these effects are much too small to explain differences of about 20 percent.

In the layer near the walls, the extra stress is described by the viscometric functions. In some distance from the walls, however, the velocity is large enough to have the rheological properties affected by the changes of the rate of strain along the stream lines; the actual shear stress τ_{rz} in this region might be lower than in the GNF power law solution, where the shear stress is calculated with the local shear rates. If this explains the low values of the measured pressures in *div*erging radial flow, experiments in *con*verging radial flow should give pressure drops larger than calculated with the GNF power law solution.

ACKNOWLEDGMENT

The author thanks Professor R. B. Bird for supporting this research, for many helpful discussions, and for critical comments. The numerical calculations have been done with the National Science Foundation Grant No. GK-24749 to Professor Bird. The author also thanks the Deutsche Forschungs Gemeinschaft for financial support during the stay at the University of Wisconsin, Madison.

NOMENCLATURE

a = thermal diffusivity, m^2/sec
$b = -1/\eta\ (\partial\eta/\partial T)_{\dot\gamma}$ = temperature coefficient of viscosity, $°K^{-1}$
c = specific heat capacity, J/kg°K
$f(z)$ = function (see *Eq 1*) [m^2sec^{-1}], $f' = df/dz$; $f'' = d^2f/dz^2$
Gz = Graetz number (see *Eq 28*)
GNF = generalized Newtonian fluid
h = gap width of radial flow channel, m
k = thermal conductivity, J/msec°K
m, n = see *Eq 11*
$m'\ n'$ = see *Eq 12*
m'', n'' = see *Eq 12*
Na = Nahme number (see *Eq 27*)
p = pressure, N/m^2
Q = volume flow rate, m^3/sec
r = radius, m
r_o, R = inner and outer radius respectively, m
T = temperature, °C
v, v_r = velocity
$\bar{\bar{v}}_r$ = reference velocity (see *Eq 25*)
z = coordinate
β = second normal stress coefficient, $Nm^{-2}sec^2$
$\dot{\bar{\bar{\gamma}}}$ = rate of strain tensor, sec^{-1}
$\bar{\bar{\gamma}}_{rz}, \dot\gamma$ = shear rate, sec^{-1}
η = shear viscosity, $Nm^{-2}sec$
$\bar\eta$ = reference viscosity (sec *Eq 26*), $Nm^{-2}sec$
θ = coordinate
θ = first normal stress coefficient, $Nm^{-2}sec^2$ } respectively
ρ = density, kgm^{-3}
τ = extra stress tensor, Nm^{-2}
$\bar{\bar{\tau}}$

Indices
w = at upper wall ($z = +h/2$)
R = at outer radius ($r = R$)

REFERENCES

1. R. B. Bird, W. E. Stewart, and E. N. Lightfoot, "Transport Phenomena," pp. 106, 114, New York, London, Sidney (1960).
2. T. Y. Na and A. G. Hansen, *Int. J. Non-Linear Mech.* 2, 261 (1967).
3. J. R. A. Pearson, "Mechanical Principles of Polymer Melt Processing," p. 128, Pergamon Press (1966).
4. M. R. Kamal and S. Kenig, *Polym. Eng. Sci.*, 12, 294 (1972).
5. J. L. Berger and C. G. Gogos, *Polym. Eng. Sci.*, 13, 102 (1973).
6. B. R. Laurencena and M. C. Williams, *Trans. Soc. Rheol.*, 18, 331 (1974).
7. W. H. Schwarz and C. Bruce, *Chem. Eng. Sci.*, 24, 399 (1969).
8. J. M. Piau and M. Piau, *C. R. Acad. Sc. (Paris)*, 269, 1214 (1969) and 270, 159 (1970).

9. W. O. Criminale, J. L. Erickson, and G. L. Filbey, *Arch. Rational Mech. Anal.*, 1, 410 (1958).
10. J. L. Livesey, *Int. J. Mech. Sci.*, 1, 84 (1960).
11. S. B. Savage, *Trans. Am. Soc. Mech. Eng.*, 31, 594 (1964).
12. O. K. Bertsch, *Untersuchung der Druckverteilung bei radialter Strömung zwischen zwei parallelen Platten*, exp. Studienarbeit, Inst. f. Kunststofftechnologie Universität Stuttgart (1973).
13. K. H. Hellwege, W. Knappe, and P. Lehmann, *Kolloid-Z.* 183, 110 (1962).
14. G. Schenkel and G. Robens, *Messung der rheologischen Stoffwertfunktionen für die Kunststoffverarbeitung*, DFG-Forschungsvorhaben Nr. 2463 (1972-73).
15. R. B. Bird, O. Hassager, and S. I. Abdel-Khalik, *AIChE J.*, 20, 1041 (1974).
16. J. Meissner, *Proc. Fourth Int. Cong. Rheol., 1963*, p. 437, Interscience Publishers, New York (1965).
17. K. Higashitani and W. G. Pritchard, *Trans. Soc. Rheol.*, 16, 687 (1972).
18. H. H. Winter, *Polym. Eng. Sci.*, 15, 84 (1975).